versed by restoration of neutrality, although the refolded Mediator appeared slightly different from the original compact form.

The related murine complex, containing homologs of yeast Mediator subunits (*6*), appeared similar to yeast Mediator in the electron microscope. Fields of well-defined particles gave evidence of a discrete complex, and selection, alignment, and averaging yielded a view in projection. The murine complex was not only the same size and shape as yeast Mediator but also bore a close resemblance in internal structural detail (Fig. 4). The very occurrence of such a view, deriving from a preferred orientation on the surface of the electron microscope grid, points to a similarity in 3D structure of the two complexes, leading to a similar manner of adsorption to the grid.

The murine complex also underwent a conformational change to an extended form at high pH or in the presence of RNA polymerase II (*14*). Unfolding was again species specific, occurring only with mammalian but not with yeast RNA polymerase II. The proportion of extended particles was, however, smaller, and the images of holoenzyme were more variable, precluding alignment and averaging. The similarity to yeast holoenzyme was nonetheless apparent from views of individual particles.

Parallel investigation of the murine and yeast complexes was of particular interest because of the apparent differences between them. Although four components of the murine complex are homologous to yeast Mediator subunits, there is as yet no evidence of further homology, with a murine equivalent of the Sin4/Rgr1 repression-activation module being conspicuously lacking (*6*). The structural similarities noted here point to a correspondence between the two complexes: Both occur in a compact conformation of about the same size and shape and exhibit similar internal structural detail; both unfold to an extended conformation at elevated pH or in the presence of RNA polymerase II; and both interact with polymerase in the extended conformation, forming holoenzymes that are similar in general appearance. Moreover, both complexes include a tail domain, as identified in a preliminary study of yeast Mediator from a *sin4* deletion strain as the Sin4/Rgr1 repression-activation module (*15*). Thus, the murine complex appears to be a true counterpart of yeast Mediator.

Unfolding of Mediator in the presence of RNA polymerase II may reflect the equilibrium association of the two proteins detected previously by biochemical means (*16*). Mediator unfolds upon binding polymerase and fails to refold immediately after dissociation. The evidence for at least two sites of interaction with polymerase was unexpected. It was previously thought that the interaction occurred solely through the polymerase CTD. The species specificity of Mediator unfolding, as well as its persistence in the absence of the CTD, provide evidence for a second site. Apparently both sites are required for a stable interaction.

References and Notes

1. P. M. Flanagan, R. J. Kelleher III, M. H. Sayre, H. Tschochner, R. D. Kornberg, *Nature* **350**, 436 (1991).
2. Y. J. Kim, S. Bjorklund, Y. Li, M. H. Sayre, R. D. Kornberg, *Cell* **77**, 599 (1994).
3. C. M. Thompson, A. J. Koleske, D. M. Chao, R. A. Young, *ibid.* **73**, 1361 (1993).
4. Y. Li *et al.*, *Proc. Natl. Acad. Sci. U.S.A.* **92**, 10864 (1995).
5. L. C. Myers *et al.*, *Genes Dev.* **12**, 45 (1998).
6. Y. W. Jiang *et al.*, *Proc. Natl. Acad. Sci. U.S.A.* **95**, 8538 (1998).
7. L. C. Myers, K. Leuther, D. A. Bushnell, C. M. Gustafsson, R. D. Kornberg, *METHODS: A Companion to Methods in Enzymology* **12**, 212 (1997).
8. Purified Mediator was assayed in reactions reconstituted with essentially pure transcription proteins (*7*). Maximal transcriptional activation and maximal stimulation of basal transcription were obtained with levels of Mediator that were less than stoichiometric with core RNA polymerase II, which is indicative of a high percentage of active Mediator molecules.
9. About 85% of the particles were clearly recognizable as belonging to the reported average conformation and orientation. Most of the remaining particles appeared to be distorted but were easily recognized as variants of the average, most likely affected by the sample preparation procedure (adsorption to the grid and negative staining).
10. J. Frank *et al.*, *J. Struct. Biol.* **116**, 190 (1996).
11. The resolution of all average projection maps, calculated by Fourier ring correlation analysis of partial averages (*10*), was about 40 Å.
12. S. A. Darst, A. M. Edwards, E. W. Kubalek, R. D. Kornberg, *Cell* **66**, 121 (1991).
13. G. D. Meredith *et al.*, *J. Mol. Biol.* **258**, 413 (1996).
14. F. J. Asturias, Y. W. Jiang, L. C. Myers, C. M. Gustafsson, R. D. Kornberg, data not shown.
15. F. J. Asturias *et al.*, unpublished data.
16. J. Q. Svejstrup *et al.*, *Proc. Natl. Acad. Sci. U.S.A.* **94**, 6075 (1997).

17. Supported by NIH grants AI21144 and GM36659 to R.D.K.

5 October 1998; accepted 7 January 1999

Crystallographic Evidence for Preformed Dimers of Erythropoietin Receptor Before Ligand Activation

Oded Livnah,[1*] Enrico A. Stura,[1†] Steven A. Middleton,[2] Dana L. Johnson,[2] Linda K. Jolliffe,[2‡] Ian A. Wilson[1‡]

Erythropoietin receptor (EPOR) is thought to be activated by ligand-induced homodimerization. However, structures of agonist and antagonist peptide complexes of EPOR, as well as an EPO-EPOR complex, have shown that the actual dimer configuration is critical for the biological response and signal efficiency. The crystal structure of the extracellular domain of EPOR in its unliganded form at 2.4 angstrom resolution has revealed a dimer in which the individual membrane-spanning and intracellular domains would be too far apart to permit phosphorylation by JAK2. This unliganded EPOR dimer is formed from self-association of the same key binding site residues that interact with EPO-mimetic peptide and EPO ligands. This model for a preformed dimer on the cell surface provides insights into the organization, activation, and plasticity of recognition of hematopoietic cell surface receptors.

Erythropoietin (EPO) is a glycoprotein hormone that regulates the proliferation, differentiation, and maturation of erythroid cells (*1*). The EPO receptor (EPOR), a member of the class 1 cytokine receptor superfamily (*2*), consists of an extracellular ligand-binding domain, a short single-pass transmembrane segment, and a cytoplasmic domain that lacks a kinase region (*3*). Signaling occurs through the JAK/STAT pathway, where ligand-induced sequential receptor homodimerization (*4–6*) has been proposed to promote stable association of JAK2 and phosphorylation of JAK2, EPOR, and STAT5 (*7*). EPOR can also be activated through a point mutation in the extracellular region (EPO binding protein, EBP) that produces a disulfide-linked homodimer (*5*), by a small percentage of monoclonal antibodies to EPOR (*8*) and by a set of short EPO-mimetic peptides (*9*) (EMPs) that are unrelated in sequence to EPO and can be considered minimized hormones (*9*, *10*). The crystal structure of an agonist EMP1-EBP complex (*11*) revealed a two-

[1]Department of Molecular Biology and Skaggs Institute of Chemical Biology, The Scripps Research Institute, 10550 North Torrey Pines Road., La Jolla, CA 92037, USA. [2]R. W. Johnson Pharmaceutical Research Institute, Drug Discovery Research, 1000 Route 202, Box 300, Raritan, NJ 08869, USA.

*Present address: Department of Biological Chemistry, Institute of Life Sciences, Wolfson Centre for applied Structural Biology, Hebrew University of Jerusalem, Jerusalem 91904, Israel.

†Present address: Department d'Ingenierie et d'Etude des Proteines, BAT 152 C.E.A./SACLAY, 91191 Gif sur Yvette Cedex, France.

‡ To whom correspondence should be addressed.

Table 1. Crystallographic data and refinement statistics for the native EBP. The unliganded EBP (7 mg/ml) was crystallized by sitting drop vapor diffusion at 22.5C with 0.84 to 0.9 M ammonium sulfate and 0.1 M imidazole (pH 7.8). These conditions differ from those used for the EMP1-EBP complex (*11*), which crystallizes from 11% MPEG 5000 (monomethyl ether) and 0.2 M imidazole malate (pH 7.7) with peptide at 1 to 2 mg/ml. Crystals of the native EBP are triclinic *P*1, with cell parameters a = 38.8 Å, b = 55.7 Å, c = 58.4 Å, α = 62.7, β = 88.3, γ = 75.0°, with two EBP molecules in the asymmetric unit and a V_M (Matthews coefficient) of 1.97 Å^3 per dalton. Data were collected from a single crystal at the Stanford Synchrotron Radiation Laboratory beam line 7-1 at −180°C. The data were integrated, scaled, and reduced with DENZO and SCALEPACK (*30*), and the structure was determined by molecular replacement methods with AMoRe (*30*), as implemented in the CCP4 program suite (*30*). The search models used were the individual D1 and D2 domains of the EBP molecule (*11*) from the EBP-EMP1 complex (PDB code 1EBP). The molecular replacement solution revealed an EBP dimer in the asymmetric unit (R_{cryst} = 44%, correlation coefficient = 43%). The structure was initially refined by rigid body searches with X-PLOR 3.851 (*30*) at a resolution range of 8.0 to 4.0 Å (R_{cryst} and R_{free} = 41%) and further refined by the simulated annealing slow-cooling protocol in the resolution range of 50 to 2.4 Å. The F_{obs} factors were scaled anisotropically ($B11$ = −2.2 Å^2; $B12$ = −3.6 Å^2; $B22$ = −4.4 Å^2; $B13$ = 2.5 Å^2; $B23$ = 0.1 Å^2; $B33$ = 4.7 Å^2) and a bulk solvent correction was applied (*30*). The structure was fitted into the electron density maps with the graphics program O (*30*). Residues 1 to 9, 21 to 23, 135, 164, and 222 to 225 of EBP monomer 1 and residues 1 to 9, 21 to 23, 164, and 223 to 225 of monomer 2 had insufficient electron density to be refined, as observed in other EBP structures (*11–13*). In the final structure, none of the nonglycine residue lie in the disallowed region of the Ramachandran plot as analyzed with PROCHECK (*30*). Symbols: See (*31*).

Resolution range	50 to 2.4 Å
Unique reflections	14,951
Redundancy	2.0
R_{sym} (I)	5.9% (28%)*
Completeness	98.6% (97.0%)*
$\langle I/\sigma(I)\rangle$	9.3 (2.1)*
Number of protein atoms	3240
Number of solvent atoms	97
R_{cryst} ($F > 1\sigma_F$)	21.6
R_{free}	29.6
rmsd from ideality	
Bond length	0.008 Å
Bond angle	1.6 Å
Dihedrals	24.4 Å
Improper dihedrals	0.8 Å
Average B values	
EBP monomer 1	32 Å^2
EBP monomer 2	33 Å^2
Ramachandran plot (PROCHECK)	
Favored	81.5%
Allowed	17.0%
Generously allowed	1.4%
Disallowed	0.0%

*Statistics for outer shell of 2.5 to 2.4 Å data.

fold symmetric dimer assembly (Fig. 1), whereas an antagonist peptide (EMP33) produces an asymmetric dimer that is apparently not permissive for JAK2 phosphorylation (*12*). These results, combined with the highly asymmetric EPO-EPObp structure (*13*), suggest that receptor dimer orientation affects EPOR activation.

EBP, consisting of residues 1 to 225 of the human EPOR, was expressed and purified as described (*14*). The crystal structure of native, unliganded EBP was determined at 2.4 Å resolution by molecular replacement (Table 1). Each EBP monomer (*15*) consists of two FBN-III folds (D1 and D2), connected at an approximate right angle, as in other cytokine receptors (*16*). However, the native EBP unexpectedly forms a cross-shaped dimer (Fig. 1A). The self-dimer interface (*17*) (Figs. 1 and 2A) involves an almost perfect twofold symmetric interaction of 24 residues from five of the six binding loops L1, L3, L4, L5, and L6 (*18*) and a small loop segment (L5a) between strand C′ and E in D2 (Fig. 2B) that are markedly similar to those used to bind EPO (Fig. 2C). A hydrophobic core includes two layers, from four aromatics, Phe^{93} (L3), and Phe^{205} (L6) of each EBP that form a crownlike ring structure, reminiscent of the hydrophobic interface between

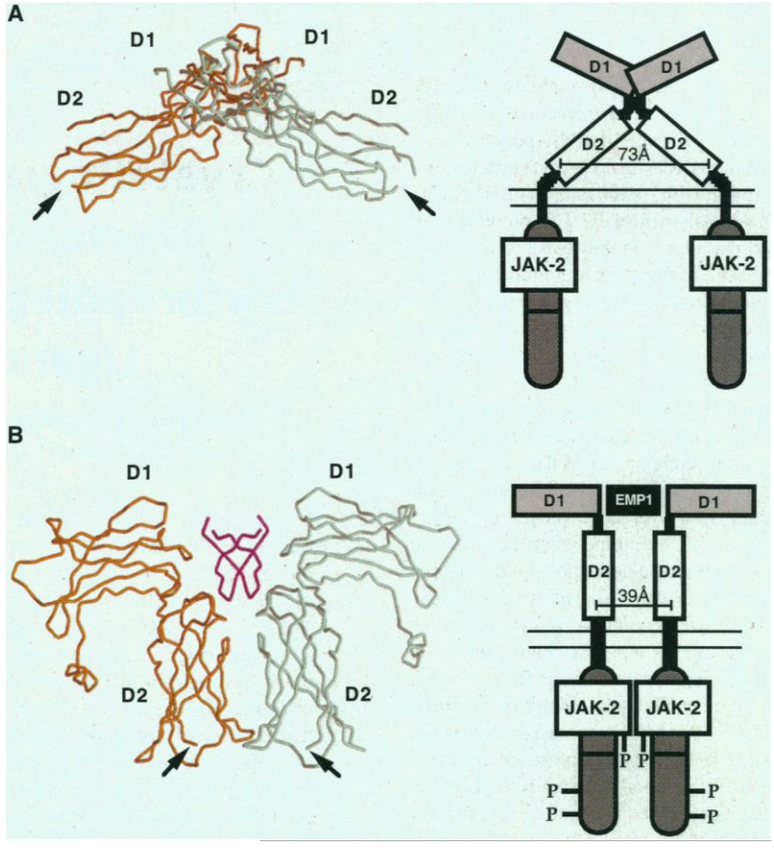

Fig. 1. Comparison of the unliganded and liganded EPOR receptor dimer configurations. (**A**) A schematic representation of the quaternary structure of the native EBP dimer. The two EBP molecules form a cross-like self dimer and are shown in cyan and gold, with their individual domains labeled D1 and D2. A close, symmetrical interaction is formed between the two EBP molecules on the basis of their previously determined ligand-binding epitope regions (*11*). The three-residue linker between the NH_2-terminal α helix and the FBN-III domains in both molecules is omitted because of the lack of electron density in this region and the NH_2-terminal α helices are omitted for clarity. The D1 domains of each monomer point in opposite directions, whereas the two D2 domains can both be aligned toward the membrane with a rotation of 135° between them. The membrane-proximal ends of D2 in each molecule (Thr^{220}) are shown by a black arrow emphasizing the 73 Å separation between them. In the schematic of the unliganded self dimer (right), the different scissors-like dimer configuration keeps the intracellular ends far enough apart such that autophosphorylation of JAK-2 cannot occur and hence other phosphorylation events, such as on the cytoplasmic domain of the EPOR, do not occur. (**B**) The quaternary structure of the EBP-EMP1 complex. The two EBP molecules are shown in gold and cyan and the EMP1 dimer in purple. Two EMP1 peptides bind to two EBP receptor molecules in a symmetrical manner (*11*). The domains are labeled in D1 and D2 and the equivalent COOH-terminal membrane-proximal ends of each receptor are shown by black arrows that highlight the difference in distances and receptor dimer configurations for the unliganded native and EMP1-complexed EBPs. In the schematic of the liganded form (right), EMP1 [or EPO (*13*)] induces a close dimer association of both the D1 and D2 domains so that their intracellular regions become substrates for phosphorylation by two JAK-2 molecules. The stick figures were made with MIDAS (*30*).

EMP1 and EBP (*11*), and from Leu[33] (L1), Pro[149] (L5), and Met[150] (L5). A large number of polar residues provide sufficient hydrogen bonding (*19*) to fix the geometry of the quaternary association.

Comparison of the native and EBP-EMP1 structures shows that the D2 domain of the unliganded EBP is rotated toward D1 by 13°, so that a relative shift of 8 Å is observed at the distal edge of D2 (*20*). Thus, some flexibility in the interdomain angle is observed, as in other cytokine receptors (*21*). Two ligand-binding loops (L3 and L6) show large conformational changes (*22*), compared with the EMP1 complex, and contain the "hot spot" residues Phe[93] and Phe[205] that are essential for binding EPO and EMP1 (*11*, *23*). The EBP-EBP receptor contact residues are markedly similar to those used for binding EMP1 (*11*), EMP33 (*12*), and EPO (*13*) (Fig. 2). The two equivalent COOH-terminal residues (Thr[220]), adjacent to the predicted point of membrane insertion, are 39 Å and 73 Å apart for the EMP1-EBP and EBP-EBP structures, respectively, which would keep the EBP-EBP self-dimer cytoplasmic domains sufficiently separated to prevent association of the two JAK2 molecules and, hence, would inhibit a background signaling (Fig. 1). Ligand binding would bring the D2 domains closer together, possibly by a scissors-type motion, and facilitate interaction of their intracellular domains.

Although ligand-induced receptor dimerization is widely accepted as a prerequisite for EPOR activation, it has not been clear whether the unliganded receptors would self-associate on the cell surface. However, additional support for EPOR dimers can be gleaned from studies of EPOR biology. Monomeric EPO binding to dimeric EPOR involves a two-site mechanism, with high-affinity (nanomolar range) and low-affinity (micromolar range) sites (*6*). A self-associated EPOR dimer would explain how EPO can activate efficiently on the cell surface where relatively few receptors (<1000) are present (*24*). Without some clustering of receptors, even transitory, monomeric receptor-EPO interactions would be prevalent, especially in an excess of EPO. Indeed, clustering of receptors, such as by homodimerization, has been proposed to account for the low numbers of expected EPO:EPOR dimers as a result of the low affinity of the second site and the low level of 1 μM receptor on the cell surface (*6*). However, detection of such dimers in solution would be complicated by the expected weak association (millimolar range) of the truncated soluble, extracellular forms of cell surface receptors (*25*). However, these affinities could easily translate into the micromolar range on the cell surface as a result of two-dimensional lateral diffusion (*25*) and increased stability of the full-length receptor containing the transmembrane domain (*26*). Indeed, even a 50 mM dissociation constant would provide sufficient clustering of receptors to substantially enhance the low-affinity second-site EPO-EPOR interaction (*6*).

In order to test the biological relevance of the crystallographic EPOR self-dimer, experiments were designed by Remy *et al.* (*27*) to determine the association state of the unliganded receptor on the cell surface. These fluorescent protein fragment complementation assays readily detect distinct dimeric EPOR configurations for liganded and unliganded EPOR on

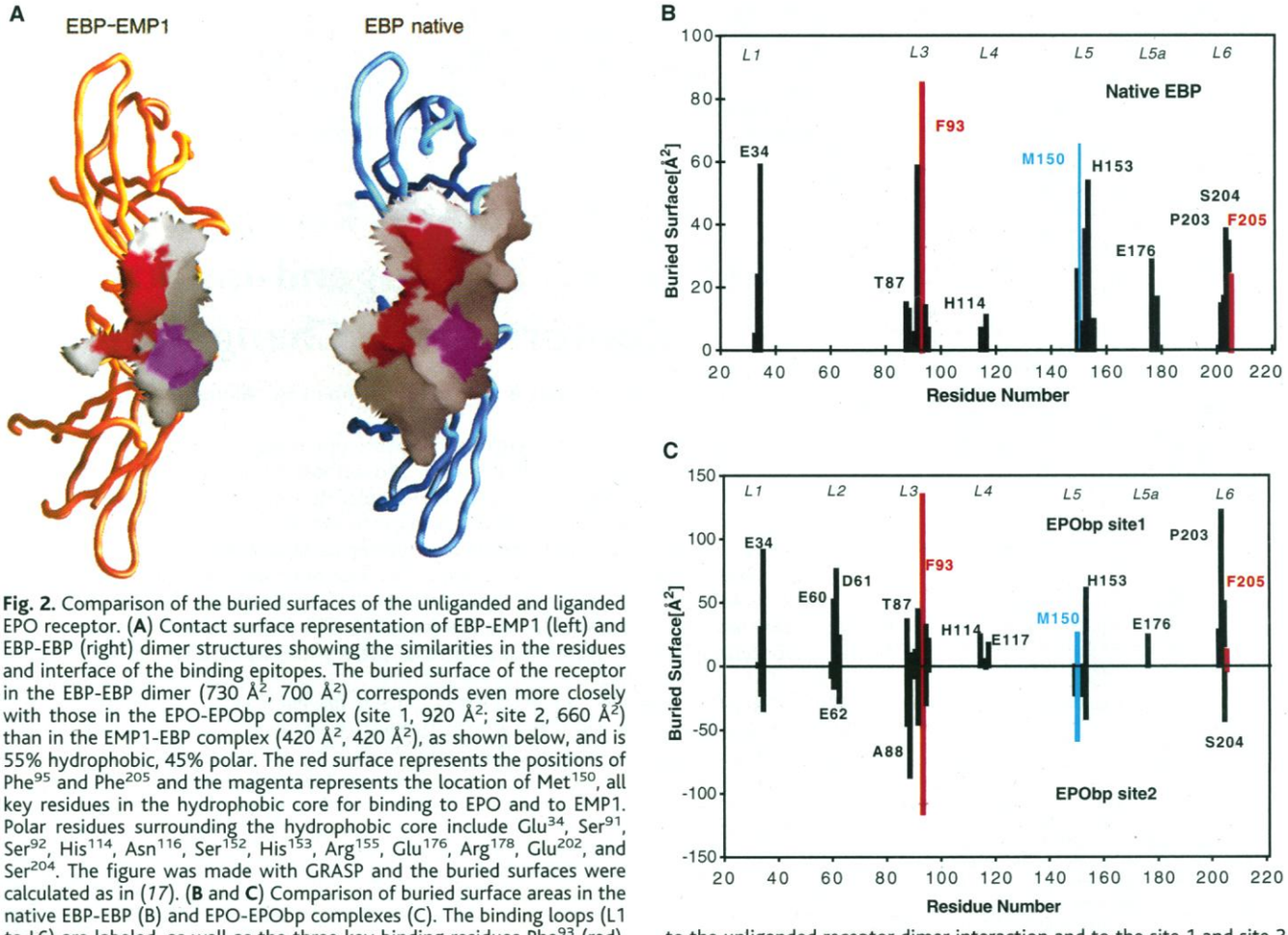

Fig. 2. Comparison of the buried surfaces of the unliganded and liganded EPO receptor. (**A**) Contact surface representation of EBP-EMP1 (left) and EBP-EBP (right) dimer structures showing the similarities in the residues and interface of the binding epitopes. The buried surface of the receptor in the EBP-EBP dimer (730 Å², 700 Å²) corresponds even more closely with those in the EPO-EPObp complex (site 1, 920 Å²; site 2, 660 Å²) than in the EMP1-EBP complex (420 Å², 420 Å²), as shown below, and is 55% hydrophobic, 45% polar. The red surface represents the positions of Phe[95] and Phe[205] and the magenta represents the location of Met[150], all key residues in the hydrophobic core for binding to EPO and to EMP1. Polar residues surrounding the hydrophobic core include Glu[34], Ser[91], Ser[92], His[114], Asn[116], Ser[152], His[153], Arg[155], Glu[176], Arg[178], Glu[202], and Ser[204]. The figure was made with GRASP and the buried surfaces were calculated as in (*17*). (**B** and **C**) Comparison of buried surface areas in the native EBP-EBP (B) and EPO-EPObp complexes (C). The binding loops (L1 to L6) are labeled, as well as the three key binding residues Phe[93] (red), Phe[205](red), and Met[150] (cyan) and others that contribute substantially to the unliganded receptor dimer interaction and to the site 1 and site 2 interactions in the EPO-EPObp complex [data from (*13*)].

living cells and strongly support our model of ligand-induced reorganization of the EPOR dimer (*27*). EPOR, and perhaps other cytokine receptors (*28*), would then exist as unliganded dimers on the cell surface. The hormone would trigger a switch between a self-associated, inactive conformation and an active, ligand-bound conformation. Agonists and antagonists would then have to consider self association as a competing reaction, but small-molecule antagonists for this family of receptors could now be designed to stabilize the inactive dimeric form. Finally, plasticity of receptor binding sites in ligand recognition is emerging as a prevalent theme throughout biology (*21*, *29*). The structure of the human growth hormone receptor initially showed that the same receptor binding site residues interact with completely different faces of its hormone ligand (*16*). In the EPOR system, the same binding site interacts with two sites on EPO (*13*), various EMPs (*11*, *12*), and now with itself.

References and Notes

1. S. B. Krantz, *Blood* **77**, 419 (1991); K. Jacobs *et al.*, *Nature* **313**, 806 (1985).
2. J. A. Wells and A. M. de Vos, *Annu. Rev. Biochem.* **65**, 609 (1996); J. F. Bazan, *Proc. Natl. Acad. Sci. U.S.A.* **87**, 6934 (1990).
3. M. Murakami *et al.*, *Proc. Natl. Acad. Sci. U.S.A.* **88**, 11349 (1991); N. Jiang, T. C. He, A. Miyajima, D. M. Wojchowski, *J. Biol. Chem.* **271**, 16472 (1996).
4. O. Miura and J. N. Ihle, *Arch. Biochem. Biophys.* **306**, 200 (1993); D. L. Barber, J. C. DeMartino, M. O. Showers, A. D'Andrea, *Mol. Cell. Biol.* **14**, 2257 (1994); D. J. Matthews, R. S. Topping, R. T. Cass, L. B. Giebel, *Proc. Natl. Acad. Sci. U.S.A.* **93**, 9471 (1996).
5. S. S. Watowich *et al.*, *Proc. Natl. Acad. Sci. U.S.A.* **89**, 2140 (1992); S. S. Watowich, D. J. Hilton, H. F. Lodish, *Mol. Cell. Biol.* **14**, 3535 (1994).
6. J. S. Philo, K. H. Aoki, T. Arakawa, L. Owens-Narhi, J. Wan, *Biochemistry* **35**, 1681 (1996).
7. B. A. Witthuhn *et al.*, *Cell* **74**, 227 (1993); O. Miura *et al.*, *Blood* **84**, 1501 (1994).
8. S. Elliott, T. Lorenzini, D. Yanagihara, D. Chang, G. Elliott, *J. Biol. Chem.* **271**, 24691 (1996); H. Schneider *et al.*, *Blood* **89**, 473 (1997).
9. N. C. Wrighton *et al.*, *Science* **273**, 458 (1996).
10. D. L. Johnson *et al.*, *Biochemistry* **37**, 3699 (1998).
11. O. Livnah *et al.*, *Science* **273**, 464 (1996).
12. O. Livnah *et al.*, *Nature Struct. Biol.* **5**, 993 (1998).
13. R. S. Syed *et al.*, *Nature* **395**, 511 (1998).
14. D. L. Johnson *et al.*, *Protein Expr. Purif.* **7**, 104 (1996).
15. The two independent EBP monomers of the dimer have a root mean square deviation (rmsd) of 0.52 Å for all Cα.
16. A. M. de Vos, M. Ultsch, A. A. Kosiakoff, *Science* **255**, 306 (1992); M. Sundstrom *et al.*, *J. Biol. Chem.* **271**, 32197 (1996); W. Somers *et al.*, *Nature* **372**, 478 (1994); M. R. Walter *et al.*, *ibid.* **376**, 230 (1995).
17. M. L. Connolly, *J. Appl. Crystallogr.* **16**, 548 (1983); *ibid.* p. 439. The buried surface calculations were carried out by the program MS with a probe radius of 1.7 Å.
18. The L2 loop is a common component of the binding determinants in the cytokine receptor superfamily (*13*, *16*) but is located in the most distal part of the receptor NH_2-terminal D1 domain between strands C and C′. Thus, in the crystal structures of EBP with the smaller EMP peptide ligands (*11*) and the native EBP, L2 does not participate in ligand binding.
19. Hydrogen bonds are made, for example, between His^{153} imidazole (L5) with the backbone amide of Leu^{33} and the Glu^{34} carboxyl (L1), the main chain amide of Phe^{93} (L3) with the Ser^{204} hydroxyl (L6), and Glu^{176} carboxyl (L5a) with Ser^{91} hydroxyl (L3).
20. Superposition of the individual D1 and D2 domains of the native and EBP-EMP1 structures gives rmsd's of 0.92 Å (90 pairs) and 1.2 Å (98 pairs), respectively, for the Cα atoms.
21. S. Atwell, M. Ultsch, A. M. de Vos, J. A. Wells, *Science* **278**, 1125 (1997); T. Clackson, M. H. Ultsch, J. A. Wells, A. M. de Vos, *J. Mol. Biol.* **277**, 1111 (1998); M. Huang *et al.*, *ibid.* **275**, 873 (1998).
22. L3 undergoes the largest change such that the relative position of Phe^{93} is shifted 3.0 Å and 4.3 Å for its Cα and phenyl ring, respectively. L6 undergoes shifts of 1.1 Å and 0.9 Å for the Cα and phenyl ring, respectively, but the position of Phe^{205} remains relatively unperturbed.
23. F. P. Barbone *et al.*, *J. Biol. Chem.* **272**, 4985 (1997); L. K. Jolliffe *et al.*, *Nephrol. Dial. Transplant.* **10**, 28 (1985); S. A. Middleton *et al.*, *J. Biol. Chem.* **271**, 14045 (1996); S. A. Middleton *et al.*, in preparation.
24. K. Sawada, S. B. Krantz, S. T. Sawyer, C. I. Civin, *J. Cell. Physiol.* **137**, 337 (1988); K. Sawada *et al.*, *J. Clin. Invest.* **80**, 357 (1987); V. C. Broudy, N. Lin, M. Brice, B. Nakamoto, T. Papayannopoulou, *Blood* **77**, 2583 (1991).
25. N. L. Thompson *et al.*, *Photochem. Photobiol.* **65**, 39 (1997).
26. D. Langosch *et al.*, *J. Mol. Biol.* **263**, 525 (1996); B. Brosig and D. Langosch, *Protein Sci.* **7**, 1052 (1998); R. Laage and D. Langosch, *Eur. J. Biochem.* **249**, 540 (1997).
27. I. Remy, I. A. Wilson, S. W. Michnick, *Science* **283**, 990 (1999).
28. J. H. Naismith, T. Q. Devine, B. J. Brandhuber, S. R. Sprang, *J. Biol. Chem.* **270**, 13303 (1995); J. H. Naismith, T. Q. Devine, T. Kohno, S. R. Sprang, *Structure* **4**, 1251 (1996); J. H. Naismith, B. J. Brandhuber, T. Q. Devine, S. R. Sprang, *J. Mol. Recognit.* **9**, 113 (1996). These studies propose a related model for tumor necrosis factor receptor 1 (TNF-R1) in which the unliganded extracellular domains of the receptor may exist as a dimer on the membrane surface, and their cytoplasmic domains would then be separated by more than 100 Å. It has been unclear if this configuration exists in vivo because crystal structures of the TNF-soluble TNF receptor [D. W. Banner *et al.*, *Cell* **73**, 431 (1993)] have shown that the stoichiometry of the ligand bound receptor is 3:3. However, in light of our EPOR studies, the TNF-R1 unliganded structure may indeed be biologically relevant.
29. The interaction of an antibody with both its protein antigen and idiotypic antibody [B. A. Fields, F. A. Goldbaum, X. Ysern, R. J. Polijak, R. A. Mariuzza, *Nature* **374**, 739 (1995)] and the plasticity of the T cell receptor recognition of foreign and self MHC-peptide antigens [K. C. Garcia *et al.*, *Science* **279**, 1166 (1998)] are further examples.
30. Crystallographic programs and methods. DENZO and SCALEPACK: Z. Otwinowski and W. Minor, *Methods Enzymol.* **276**, 307 (1997); AMoRE: J. Navaza, *Acta Crystallogr.* **A50**, 157 (1994); CCP4: S. Bailey, *ibid.*, p. 760; X-PLOR: A. T. Brünger, *ibid.* **A47**, 195 (1991); A. T. Brünger, *X-PLOR, Version 3.1: A system for x-ray and NMR* (Yale Univ. Press, New Haven, CT 1992); bulk solvent: J. S. Jiang and A. T. Brünger, *J. Mol. Biol.* **243**, 100 (1994); Program O: T. A. Jones, J. Y. Zou, S. W. Cowan, M. Kjeldgaard, *Acta Crystallogr.* **A47**, 110 (1991); PROCHECK: R. A. Laskowski, M. W. MacArthur, D. S. Moss, J. M. Thornton, *J. Appl. Crystallogr.* **26**, 283 (1993); GRASP: A. Nicholls, R. Bharadwaj, B. Honig, *Biophys. J.* **64**, 166 (1993).
31. $R_{cryst} = \Sigma||F_o| - |F_c||/\Sigma F_o$, where F_o and F_c are the observed and calculated structure factors, respectively. For $\langle I/\sigma(I)\rangle$, I is the measured intensity. For R_{free}, the sum is extended over λa subset of reflections (10%) excluded from all stages of refinement (1456 reflections). $R_{sym} = \Sigma\Sigma|Ii - \langle I\rangle|/\Sigma Ii$, where $\langle I\rangle$ is the average of equivalent reflections and the sum is extended over all measured observations for all unique reflections.

32. We thank J. Gately Luz for preparation of schematics in Fig. 1, K. Hotta for help with figures, S. Michnick and J. Kelly for helpful discussions, and R. Syed and R. Stroud for providing data for Fig. 2C. Supported in part by NIH grant GM49497 (I.A.W.) and the Rueff-Wormser Scholarship Fund (O.L.). This is publication 11901-MB from The Scripps Research Institute. The unliganded EBP coordinates have been deposited in the Protein Data Bank (PDB) with the accession code 1ern.

16 September 1998; accepted 12 January 1999

Erythropoietin Receptor Activation by a Ligand-Induced Conformation Change

Ingrid Remy,[1] Ian A. Wilson,[2] Stephen W. Michnick[1]*

Erythropoietin and other cytokine receptors are thought to be activated through hormone-induced dimerization and autophosphorylation of JAK kinases associated with the receptor intracellular domains. An in vivo protein fragment complementation assay was used to obtain evidence for an alternative mechanism in which unliganded erythropoietin receptor dimers exist in a conformation that prevents activation of JAK2 but then undergo a ligand-induced conformation change that allows JAK2 to be activated. These results are consistent with crystallographic evidence of distinct dimeric configurations for unliganded and ligand-bound forms of the erythropoietin receptor.

The erythropoietin receptor (EpoR) shares both structural and functional features with the cytokine receptor superfamily that includes the interleukins, human growth hormone (hGH), and colony-stimulating factor (*1*, *2*). Crystal structures and biochemical analysis have led to the generally accepted dimerization model of growth factor–mediated receptor activation, where monomeric receptors remain inactive until ligand binds to and oligomerizes the receptors, allowing autophosphorylation of receptor-associated intracellular kinases (*3*). However, dimerization or oligomerization of receptors is a

[1]Département de Biochimie, Université de Montréal, Casier Postal 6128, succursale Centre-ville, Montréal, Québec, H3C 3J7, Canada. [2]Department of Molecular Biology and the Skaggs Institute for Chemical Biology, The Scripps Research Institute, 10550 North Torrey Pines Road, La Jolla, CA 92037, USA.

*To whom correspondence should be addressed.